JOURNAL OF CATALYSIS **174,** 52–64 (1998)
ARTICLE NO. CA971938

Effect of Chlorine on the Chemisorptive Properties of Rh/CeO_2 Catalysts Studied by XPS and Temperature Programmed Desorption Techniques

Dimitris I. Kondarides and Xenophon E. Verykios

Department of Chemical Engineering, Institute of Chemical Engineering and High Temperature Processes, University of Patras, P.O. Box 1414, GR-26500 Patras, Greece
E-mail: verykios@rea.iceht.forth.gr

Received July 8, 1997; revised October 3, 1997; accepted October 9, 1997

The effect of residual chlorine, originating from catalyst preparation methods on the chemisorptive properties of Rh/CeO_2 catalysts, is studied employing X-ray photoelectron spectroscopy (XPS) and temperature-programmed desorption (TPD) techniques on catalysts prepared using $Rh(NO_3)_3$ or $RhCl_3 \cdot H_2O$ as the metal precursor. XPS experiments show that, following reduction at 300°C, catalysts prepared from $RhCl_3 \cdot H_2O$ contain a significant amount of chlorine species (~7 at%) while about 30% of cerium exists in the Ce^{3+} state, probably due to the formation of cerium oxychloride ($Ce^{(III)}OCl$). Rhodium does not undergo complete reduction following treatment in hydrogen at 300°C; a portion of rhodium is in the Rh^+ state in Rh/CeO_2 catalyst prepared by $Rh(NO_3)_3$ while, in addition, Rh^{3+} species are also present in Rh/CeO_2 prepared by $RhCl_3 \cdot H_2O$. TPD experiments conducted following hydrogen or carbon monoxide adsorption on both catalysts in the range 25 to 300°C reveal that residual chlorine present on the ceria surface results in suppression of the capacity of the catalyst toward CO and H_2 adsorption and in changes in the relative population of the adsorbed species.

1. INTRODUCTION

The number of publications dealing with ceria-containing catalysts has increased significantly in recent years as revealed by a relevant review article (1). Noble metal (Rh, Pt, Pd) catalysts containing ceria as support or promoter are particularly important, mainly because of their applications in three-way catalysts for automotive emission control (1, 2). Noble metals are employed to reduce the amount of nitrogen oxides and carbon monoxide present in the exhaust of internal combustion engines, while ceria is added to automotive catalysts primarily for its oxygen storage capacity, which results from its ability to cycle between CeO_2 and CeO_{2-x}.

Cerium oxide-containing catalysts are sensitive to several factors, including reduction temperature, pretreatment conditions, and type of metal precursor used for the preparation of the M/CeO_2 catalysts (1). An interesting property of M/CeO_2 catalysts results from the ability of ceria to retain chlorine species on its surface when prepared from a chlorine-containing salt as the metal precursor. The presence of the chloride ions, residual from the catalyst preparation, enhances the stability of cerium in a low oxidation state with the formation of cerium oxychloride (3). It has been shown that a tetragonal CeOCl compound remains on the surface of M/CeO_2 catalysts even after reduction in hydrogen at a temperature of 600°C or higher (4, 5), influencing the chemisorptive and catalytic behavior of M/CeO_2 catalysts.

Bernal *et al.* (6–9) conducted detailed studies on the M/CeO_2 (M = Rh, Pt, and Pd) system and showed that the ceria support exerts a significant influence on the microstructure as well as on the chemisorptive and catalytic behavior of the metal crystallites. Trovarelli and co-workers (10–12) observed that Rh/CeO_2 catalysts possess a unique type of metal–support interaction which is capable of increasing the rate of CO and CO_2 hydrogenation and the rate of other types of reactions to a great extent. It was shown that the enhanced reaction rate is related to the ability of CeO_2 to form several stable CeO_{2-x} suboxides after high-temperature reduction, through the progressive depletion of oxygen-deficient phases with oxygen vacancies as predominant defects (10, 11). The presence of oxygen vacancies promotes CO_x activation by extracting oxygen.

Several studies have been conducted to identify the number and nature of CO and hydrogen species adsorbed on Rh surfaces. Hydrogen chemisorption on Rh(111) yields a single desorption peak whose maximum varies between 117 and 2°C with increasing surface coverage (13). TPD spectra of hydrogen adsorbed on Rh dispersed on several carriers commonly exhibit a second, activated hydrogen peak located between 150 and 250°C, as for example in the cases of Rh/Al_2O_3 (14) and Rh/TiO_2 (14, 15). This species has been attributed to the creation of new adsorption sites on the surface of small metal crystallites or to adsorption on sites at the metal–support interface (14). At higher adsorption temperatures, interaction of hydrogen with supported Rh often results in the appearance of a third hydrogen TPD peak originating from the carrier, following a

0021-9517/98 $25.00

spillover process. In the case of ceria-supported Rh catalysts it has been found that, in the presence of highly dispersed rhodium, ceria chemisorbs large amounts of hydrogen, even at room temperature (6), while over bare ceria temperatures higher than 200°C are necessary to activate the process (6, 9). Hydrogen can be desorbed from ceria as both H_2 (reversible adsorption) and H_2O (irreversible adsorption), the relative population of these two forms depending on the reduction temperature (9).

Carbon monoxide desorbs from Rh(111) (16, 17) and Rh(110) (18) in a single TPD peak at about 200°C while a shoulder that often appears is attributed to CO adsorbed in the bridged mode. Solymosi and Erdohelyi (19, 20) investigated the effect of the support (TiO_2, Al_2O_3, SiO_2, MgO) on the adsorption and dissociation of CO and on the reactivity of surface carbon on rhodium catalysts. The authors found that adsorption of CO on differently supported rhodium particles at room temperature produces almost identical infrared spectra and that desorption temperature of CO is practically the same for all samples ($T_{max} = 190$–200°C). During the desorption of CO, however, CO_2 is also formed at temperatures depending on the supporting material. The authors attributed the formation of CO_2 to the disproportionation of CO on rhodium (19, 20).

CO adsorption on supported Rh generally produces three distinct adsorption modes, i.e., linear bonded CO and bridge-bonded CO on Rh^0 sites as well as dicarbonyls on dispersed Rh^+ sites (21–24). Several factors have been proposed to be the driving force for the occurrence of Rh^+ gem–dicarbonyl species. The factors most frequently referred to are oxidation of Rh^0 by hydroxyl groups which intend to partially oxidize Rh^0 atoms, incomplete reduction of Rh particles containing a portion of Rh^+ sites, and dissociation of CO followed by oxidation of Rh^0 with the adsorbed oxygen formed (25–28).

The CO–Me/CeO_2 system has been investigated by several authors (29–33). White's group first reported that significant conversion of CO to CO_2 in the TPD of CO, and of CO_2 to CO in the TPD of CO_2, takes place over Pt/CeO_2 (29–31). This behavior was attributed to the reversible reaction of CO adsorbed on Pt with a lattice oxygen (or, conversely, CO_2, with an oxygen vacancy) of the support (30).

The ability of ceria to interact with hydrogen and CO makes characterization of Rh-containing catalysts by conventional techniques difficult. Benzene hydrogenation, a structure-insensitive reaction, has been employed to determine the percentage of metal exposed on low-loaded ceria supported rhodium (34). It has also been found that the hydrogen spillover process is blocked to a significant extent over Rh/CeO_2 catalysts prepared by impregnation with $RhCl_3 \cdot 3H_2O$ precursor.

In the present work, a detailed H_2 and CO chemisorption study was conducted over Rh/CeO_2 catalysts prepared with $RhCl_3$ and $Rh(NO_3)_3$ as metal precursors. The aim of the work is to evaluate the effect of chlorine species on CO and H_2 chemisorption behavior of Rh/CeO_2 catalysts. The surface chemistry occurring on the Cl-free and Cl-containing surfaces is derived from TPD-MS and XPS spectral results which reveal the nature and population of hydrogen and CO adsorbed species.

2. EXPERIMENTAL

Catalyst Preparation

Two 0.5 wt% Rh/CeO_2 catalysts were prepared using $RhCl_3 \cdot 3H_2O$ and $Rh(NO_3)_3$ as metal precursors, employing the incipient wetness impregnation method. Weighed amounts of Rh metal precursor were dissolved in 10 ml distilled water at 25°C, while 2–10 g of the carrier (Cerium IV oxide powder 99.9%, Alfa, surf. area: 3.6 m^2/g) was added to the solution under continuous stirring. The suspension was heated at 80°C to evaporate the water and the remaining slurry was dried in an oven at 110°C for 24 h. The solid residue was subsequently treated with hydrogen at 300°C for 2 h. The Cl-containing catalyst prepared using $RhCl_3 \cdot 3H_2O$ is designated as Rh/CeO_2(Cl) and the Cl-free catalyst prepared using $Rh(NO_3)_3$ as a metal precursor is designated as Rh/CeO_2(N).

For comparison purposes, unmetallized Cl-containing and Cl-free CeO_2 carriers were also prepared. Cl-containing CeO_2 was prepared by impregnation of CeO_2 with an aqueous solution of hydrochloric acid (6.34 g CeO_2 + 22.9 ml of 0.148 wt% HCl), followed by water evaporation, drying at 110°C, and reduction at 300°C as described above. Chlorine-free ceria was prepared in the same way by impregnation of CeO_2 with distilled water.

XPS Experiments

XPS spectra were carried out in a SPECS LHS 10 spectrometer employing the Mg$K\alpha$ (1253.6 eV) exciting radiation at 157.5 W. The apparatus consists of three chambers: the ultra-high vacuum (UHV) chamber, a multipurpose pretreatment chamber, and an introduction cell. The introduction cell also serves as a sample preparation cell where the sample can be treated with gases at atmospheric pressure and elevated temperatures. The sample is mounted on a transfer rod probe and can easily be transferred from one vessel to the other with little disturbance to the UHV chamber base pressure. Provisions are built into the probe for direct sample heating. Operation, recording of XPS spectra, and analysis of the raw data are carried out through a personal computer within the "SPECTRA" acquisition software supplied by the manufacturer.

The sample, in powder form, is placed in a specially designed stainless-steel holder with dimensions of 9×12 mm and height of 1 mm, and pressed at 2 tons for 10 min. The holder, containing the compressed powder, is then fixed on

the apparatus transfer rod probe, in contact with a tungsten wire which allows the temperature of the sample to be controlled by resistively heating the wire. A chromel–alumel thermocouple in contact with the sample holder enables temperature measurements.

Reduced ceria is known to be reoxidized when exposed to air, even at room temperature. Therefore, spectra of the $Rh/CeO_2(N)$ and $Rh/CeO_2(Cl)$ samples were obtained following reduction in the high-pressure introduction cell under flowing hydrogen at 300°C, for 30 min, at atmospheric pressure. After reduction the sample was cooled to room temperature under hydrogen flow, evacuated, and transferred to the UHV chamber for XPS measurements. Spectra were acquired at 25°C and a minimum background pressure of less than 3×10^{-9} mbar.

The characteristic photoemission peaks from Ce(3*d*), Rh(3*d*), O(1*s*), C(1*s*), and Cl(2*p*) core levels were recorded for each sample. Binding energies were corrected for charging by reference to adventitious carbon at 284.8 eV. To estimate the surface elemental composition of the catalysts, values of peak areas per scan were first obtained and a Shirley-type background was subtracted. Finally, normalized peak areas were obtained using empirically derived atomic sensitivity factors (35).

TPD-MS Experiments

Temperature-programmed desorption–Mass spectrometry (TPD-MS) experiments following hydrogen or carbon monoxide adsorption were carried out on the Cl-free and Cl-containing 0.5% Rh/CeO_2 catalysts and the unmetallized supports, using an apparatus which has been described in detail elsewhere (36). In a typical experiment, 350 mg of the sample is placed in a quartz microreactor and pretreated with an oxidation/reduction cycle to clean and stabilize its surface. Pretreatment includes heating under He flow to 600°C for 30 min followed by oxidation at 300°C under a flow of a 3% O_2/He mixture for 20 min. Oxidation temperature was maintained at 300°C to limit the possibility of Rh sintering. The sample is then purged with He for 15 min at the same temperature and subsequently reduced under flowing hydrogen at 300°C for 30 min. The sample is finally heated to 600°C under He flow, maintained at this temperature for 15 min, and cooled to the desired adsorption temperature, where H_2 (30 min) or 1% CO/He (15 min) adsorption occurs. It is then cooled to room temperature under a flow of the same absorbent gas, purged with He for 15 min to remove gas left in the tubing, and subsequently heated to 600°C under a flow of helium (40 cm^3/min) with a heating rate of 30°C/min. After completion of the TPD run, the sample was again subjected to the oxidation/reduction cycle mentioned above and was thus prepared for the next adsorption experiment. Analysis of the gases during TPD experiments was done by on-line mass spectrometer (Fisons, SXP Elite 300 H) equipped with a fast response inlet capillary/leak diaphragm system. MS signals at $m/z = 2$ (H_2), 18 (H_2O), 28 (CO), 32 (O_2), and 44 (CO_2) were continuously recorded. Calibration of the mass spectrometer was performed based on self-prepared gas mixtures of known composition. All gases used were of high purity provided by L' Air Liquid Hellas and were further purified employing water and/or oxygen traps.

3. RESULTS

Catalyst Characterization

The surface elemental composition of the reduced $Rh/CeO_2(N)$ and $Rh/CeO_2(Cl)$ catalysts calculated from the normalized peak areas of the Ce(3*d*), Rh(3*d*), O(1*s*), C(1*s*), and Cl(2*p*) core level spectra is shown in Table 1. Apparently, a significant amount of Cl species (7.1 at%) remains on the surface of the $Rh/CeO_2(Cl)$ sample after reduction at 300°C, in accordance with previous studies (3–5). Amounts of surface carbon are also present in both samples. The surface concentration of carbon is almost double over $Rh/CeO_2(Cl)$ compared to $Rh/CeO_2(N)$, although the catalysts were subjected to the same pretreatment conditions.

Using the values of surface atomic composition of Table 1, an estimation of the Ce/O atomic ratio can be obtained, which yields $CeO_{2.26}$ for $Rh/CeO_2(N)$ and $CeO_{1.74}$ for $Rh/CeO_2(Cl)$, for the depth probed by XPS. It is observed that the surface oxygen concentration on the Cl-free sample is higher than stoichiometric, indicating that reduction with hydrogen at 300°C leads to the formation of hydroxyl groups on its surface. On the Cl-containing sample, the Ce/O ratio indicates the existence of significant amounts of cerium in the Ce^{3+} state. The amount of surface rhodium atoms calculated from the XPS signals is 0.7 and 1.0% for $Rh/CeO_2(Cl)$ and $Rh/CeO_2(N)$, respectively.

The Ce(3*d*), O(1*s*) and Rh(3*d*) photoelectron spectra obtained from the catalysts examined are shown in Fig. 1. The Ce(3*d*) spectrum of ceria (Fig. 1A) can be resolved into eight components (3, 37–39). Peaks denoted as "v" represent the Ce $3d_{5/2}$ contribution and peaks denoted as "u" represent the Ce $3d_{3/2}$ contribution. Interpretation of the origin of these satellites is controversial and has been widely studied in the literature (37–39). As observed in

TABLE 1

Surface Elemental Composition of Rh/CeO_2 Catalysts Reduced with Hydrogen at 300°C

Catalyst	Surface composition (at%)				
	Ce	O	Rh	C	Cl
$Rh/CeO_2(N)$	28.6	64.5	1.0	5.9	—
$Rh/CeO_2(Cl)$	29.8	51.8	0.7	10.6	7.1

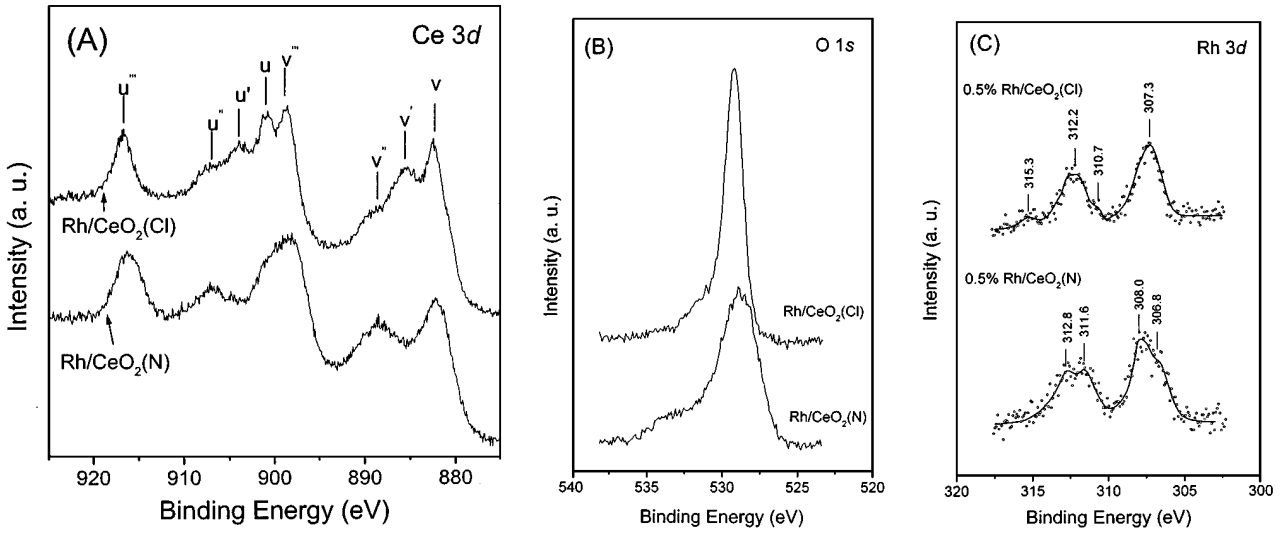

FIG. 1. Photoemission spectra of the Ce 3*d* (A), O 1*s* (B), and Rh 3*d* (C) region obtained from the $Rh/CeO_2(N)$ and $Rh/CeO_2(Cl)$ catalysts following reduction with hydrogen at 300°C.

Fig. 1A, the relative intensity of the Ce(3*d*) peaks of Cl-containing and Cl-free samples differ markedly. The v′ and u′ bands clearly observed over $Rh/CeO_2(Cl)$ are not pronounced over $Rh/CeO_2(N)$. These bands are thought to be due to the photoemission of the Ce^{3+} cation, i.e., the $3d^9 4f^1$ photoemission final state (39). On the contrary, the relative intensity of the v″(u″) and v‴(u‴) bands is higher for $Rh/CeO_2(N)$. These bands are usually assigned to the final state $3d^9 4f^0$ and are not observed for purely trivalent ionic or metallic cerium compounds (39). It can, therefore, be concluded that a significant amount of cerium in $Rh/CeO_2(Cl)$ catalyst is in the Ce^{3+} state, while in $Rh/CeO_2(N)$ the Ce^{4+} species is dominant.

It has been proposed that the relative amount of Ce^{4+} in ceria samples can be calculated from the percent area of u‴ peak in the total Ce(3*d*) region (Ce $3d_{5/2}$ and Ce $3d_{3/2}$), assuming no preferential enrichment of Ce^{4+} over Ce^{3+} or vice versa (38). This is due to the lack of the $4f^0$ configuration in the formal Ce^{3+} state. The calculated percent area of the u‴ peak so defined is shown in Table 2 for the catalysts examined. For comparison purposes, reference values for compounds containing cerium in only the Ce^{4+} or Ce^{3+} oxidation state are also given. The u‴ peak for $Ce(OH)_4$ amounts to 12.4% in the Ce(3*d*) region while for $CeAlO_3/Al_2O_3$, where cerium is in the Ce^{3+} state, the u‴ peak is absent (38). In our experiments, the u‴ peak of $Rh/CeO_2(N)$ amounts to 11.9% while for $Rh/CeO_2(Cl)$ it amounts to only 8.8% in the total Ce(3*d*) region (Table 2). Assuming a linear dependence between percent u‴ and Ce^{4+} composition it can be estimated, using the values of Table 2, that approximately 4% of the cerium atoms are in the Ce^{3+} state for $Rh/CeO_2(N)$ and 29% for $Rh/CeO_2(Cl)$, to the depth probed by XPS. The significantly higher concentration of cerium in the Ce^{3+} state observed for $Rh/CeO_2(Cl)$ is most probably due to the formation of cerium oxychloride. It has been verified (3, 4) that in Cl-containing ceria catalysts the reduced support is transformed into $Ce^{(III)}OCl$. Kepinsky *et al.* (4) found that in Cl-containing Pd/CeO_2 catalysts, CeOCl is formed in significant quantities even at reduction temperatures of 300°C and that the process is enhanced with increasing temperature of reduction (4). Similar are the results reported by Le Normand *et al.* (3).

TABLE 2

Percent Area of u‴ Peak in the Total Ce 3*d* Region (Ce $3d_{5/2}$ and Ce $3d_{3/2}$)

Sample	u‴ in Ce 3*d* (%)	Ref.	Ce^{3+} concentration (at%)
$Ce(OH)_4$	12.4	38	100
7% $CeAlO_3/Al_2O_3$	0	38	0
$Rh/CeO_2(N)$	11.9	This work	4
$Rh/CeO_2(Cl)$	8.8	This work	29

The photoemission spectra obtained from the $Rh/CeO_2(N)$ and $Rh/CeO_2(Cl)$ catalysts in the O(1*s*) region are shown in Fig. 1B. For the Cl-free sample, a broad band is observed at 528.9 eV accompanied by a high binding energy shoulder at 533.1 eV. The observed halfwidth of the main O(1*s*) peak (3.0 eV) gives evidence for the coexistence of different types of oxides, i.e., CeO_2 and Ce_2O_3. Although XPS results indicate the existence of 4% of cerium in the Ce^{3+} state (Table 2), it is probable that this value is much higher in the upper surface layer. The high-energy shoulder at 533.1 eV indicates the presence of significant amounts of hydroxyl groups terminating the ceria. The presence

of these surface hydroxyl groups explains the high stoichiometry of CeO_x, with $x = 2.26$, observed for $Rh/CeO_2(N)$ (Table 1). For Cl-containing Rh/CeO_2, the O(1*s*) is sharper and the observed halfwidth (1.5 eV) and position (529.3 eV) indicate the dominance of one type of oxide, i.e., Ce_2O_3. The small high-energy shoulder observed is probably due to residual surface peroxide groups (40). It is interesting to notice that no peak due to adsorbed hydroxyl groups is present in the O(1*s*) spectral region of $Rh/CeO_2(Cl)$.

Rhodium 3*d* photoemission peaks obtained from the Cl-free and Cl-containing Rh/CeO_2 catalysts are shown in Fig. 1C. For $Rh/CeO_2(N)$, four peaks can be distinguished, located at 306.8, 308.0, 311.6, and 312.8 eV. For pure rhodium metal foil, the Rh($3d_{5/2}$) and Rh($3d_{3/2}$) peaks occur at 307.0 and 311.8 eV, respectively, with FWHM of 1.6 eV (35). The doublet at 306.8 and 311.6 eV occurs at comparable binding energies and may, therefore, be attributed to Rh^0. The doublet observed at higher binding energies (Fig. 1C) may be attributed to rhodium particles in the Rh^+ oxidation state (42). The possibility for Rh^+ formation due to surface oxidation caused by the UHV treatment in the XPS chamber can be excluded here since in another set of experiments (not shown), where the $Rh/CeO_2(N)$ catalyst was treated with hydrogen at 500°C, no peaks due to Rh^+ were observed. The presence of Rh^+ may be due either to the incomplete reduction of rhodium at this temperature or to the oxidation of Rh^0 by surface hydroxyl groups. The latter explanation is supported by the presence of the characteristic peak of hydroxyl groups in the O(1*s*) region observed for $Rh/CeO_2(N)$ (Fig. 1B). It is evident that rhodium is not completely reduced by hydrogen at 300°C. Similar results have been reported by Baltanas *et al.* (41), who observed that Rh supported on MgO does not undergo complete reduction unless treated with hydrogen at temperatures higher than 400°C. Kawai *et al.* (42) also reported single Rh($3d_{5/2}$) peaks in their XPS spectra obtained from Rh/ZnO and Rh/MgO catalysts following reduction at 200°C, but the spectra also showed large FWHM values (>3.5 eV), which were attributed to a convoluted mixture of two oxidation states.

For $Rh/CeO_2(Cl)$ catalyst (Fig. 1C), two broad photoemission peaks due to Rh($3d_{5/2}$) and Rh($3d_{3/2}$) excitation are observed, located at 307.3 and 312.2 eV, respectively. These doublets can again be attributed to Rh^0 and Rh^+ sites, as in the case of $Rh/CeO_2(N)$. Two more peaks may also be distinguished in the spectrum of $Rh/CeO_2(Cl)$ located at 310.7 and 315.3 eV (Fig. 1C). The binding energy of this doublet is proper for Rh^{3+} species (42), indicating that Rh^{3+} sites are also present on this catalytic surface.

Concluding, the Rh(3*d*) spectra of Fig. 1C clearly show that rhodium does not undergo complete reduction after treatment with hydrogen at 300°C. Apart from Rh^0, $Rh/CeO_2(N)$ still contains rhodium in the Rh^+ electronic state while Rh^0, Rh^+, and Rh^{3+} species coexist on $Rh/CeO_2(Cl)$.

TPD-MS Experiments

TPD-MS experiments were conducted employing the Cl-free and Cl-containing 0.5% Rh/CeO_2 catalysts as well as their unmetallized supports, using the apparatus and following the procedure described in a previous section. TPD-MS spectra were obtained following hydrogen or carbon monoxide adsorption in the temperature range of 25 to 300°C.

Hydrogen Adsorption

(i) Unmetallized $CeO_2(N)$ and $CeO_2(Cl)$. The TPD-MS spectra obtained after treatment of unmetallized $CeO_2(N)$ and $CeO_2(Cl)$ samples with hydrogen at 300°C for 30 min are shown in Fig. 2. It is observed that hydrogen treatment of $CeO_2(N)$ at 300°C results in the appearance of H_2 and H_2O TPD curves which start evolving simultaneously at temperatures above 300°C. The hydrogen peak is centered at about 400°C. The fact that this peak is symmetric indicates that adsorption is linked to dissociative adsorption. The H_2O curve exhibits a broad band with a maximum located at 450°C and still desorbs at temperatures above 600°C, where the experiment is completed (Fig. 2).

On the contrary, no hydrogen is observed to desorb from similarly treated $CeO_2(Cl)$ samples. The only observed TPD peak (Fig. 2) is due to water desorption which starts evolving at about 400°C, in a lower amount compared to $CeO_2(N)$, indicating that reversible adsorption of hydrogen at 300°C is hindered over the Cl-containing sample, while irreversible adsorption is diminished.

It should be mentioned that no TPD peaks were observed after treating $CeO_2(N)$ and $CeO_2(Cl)$ samples with

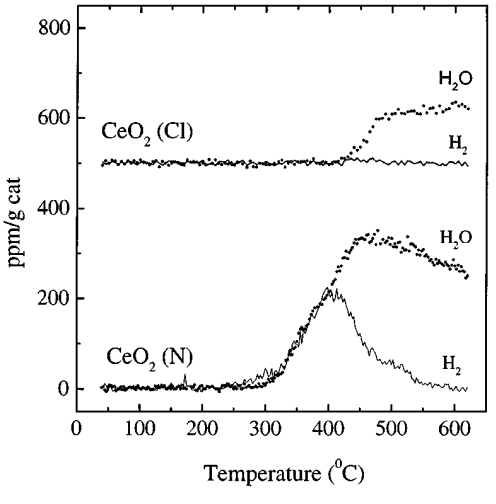

FIG. 2. TPD-MS spectra obtained following treatment of $CeO_2(Cl)$ and $CeO_2(N)$ samples with hydrogen at 300°C for 30 min.

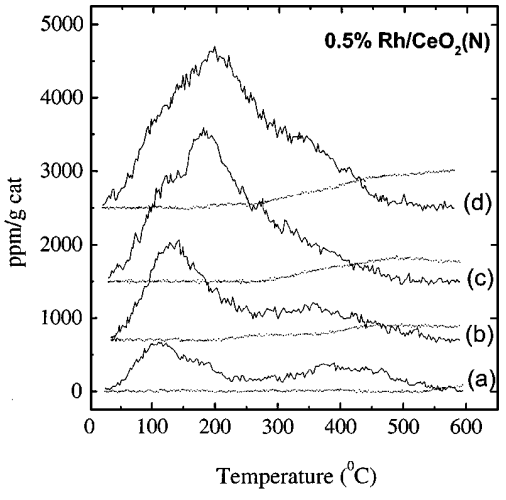

FIG. 3. TPD-MS spectra obtained following hydrogen adsorption on the 0.5% $Rh/CeO_2(N)$ catalyst for 30 min at temperatures of 25 (a), 100 (b), 200 (c), and 300°C (d). Solid lines, H_2; dotted lines, H_2O.

hydrogen at temperatures below 200°C, indicating that hydrogen interaction with ceria is an activated process. This is in accordance with the findings of Bernal *et al.* (6, 9), who observed that hydrogen chemisorption over bare CeO_2 is an activated process occurring at temperatures above 200°C.

(ii) Cl-free Rh/CeO_2. TPD spectra obtained following hydrogen adsorption on Cl-free 0.5% Rh/CeO_2 catalysts at temperatures of 25, 100, 200, and 300°C are shown in Fig. 3. Three TPD peaks due to H_2 desorption are observed, while smaller amounts of water are also produced. When hydrogen adsorption occurs at room temperature, two TPD peaks are observed below 250°C, located at 110 and 170°C, while a high-temperature broad band evolves between 300 and 550°C. The high-temperature H_2 peak evolves at the same desorption temperature as in the case of the bare $CeO_2(N)$ sample (Fig. 2), indicating that this peak possibly originates from hydrogen adsorbed on the ceria carrier. The low-temperature TPD peaks desorbing in the temperature region below 250°C may then be attributed to hydrogen adsorbed on sites linked to the presence of Rh particles.

The peak located at 170°C increases significantly in intensity upon increasing adsorption temperature. The maximum of this peak shifts from 170°C for $T_{ad} = 25$°C (Fig. 3a) to 200°C for $T_{ad} = 300$°C (Fig. 3d). This shift is accompanied by a considerable increase in the population of this species, which is the dominant one at adsorption temperatures above 200°C, indicating an activated adsorption process. The hydrogen peak located at 110°C is not significantly affected by adsorption temperature either in intensity or in location. (Fig. 3). The apparent increase in intensity is due to overlapping with the activated adsorption peak. The high-temperature peak desorbing above 300°C monotonically increases in intensity upon increasing adsorption temperature and shifts to lower temperatures. The total amount of hydrogen desorbed from $Rh/CeO_2(N)$ as a function of adsorption temperature is shown in Table 3.

TABLE 3

Amount of Hydrogen Desorbed from the 0.5% Rh/CeO_2 Catalysts Following Hydrogen Adsorption in the Temperature Range 25–300°C

Adsorption temperature (°C)	Amount of desorbed H_2 (μmol/g cat)	
	$Rh/CeO_2(N)$	$Rh/CeO_2(Cl)$
25	8.4	4.5
100	13.8	7.2
200	24.0	13.8
300	26.8	15.7

Amounts of H_2O are also observed to desorb in addition to hydrogen from Cl-free Rh/CeO_2 (Fig. 3). Although no water desorbs following hydrogen adsorption at room temperature (Fig. 3a), increasing adsorption temperature to 100, 200, and 300°C results in the appearance of H_2O-TPD curves which start evolving at 400, 300, and 250°C, respectively, in increasing amounts (Figs. 3b–3d). Since no water was observed to desorb from the unmetallized $CeO_2(N)$ carrier at adsorption temperatures lower than 200°C, these observations indicate that the Rh particles favor the formation of significant amounts of hydroxyl groups on the ceria surface upon treatment with hydrogen, even at temperatures of 100°C, which desorb as water in subsequent TPD experiments.

(iii) Cl-containing Rh/CeO_2. The corresponding TPD spectra obtained from the Cl-containing 0.5% Rh/CeO_2 catalysts are shown in Fig. 4. Again, three hydrogen peaks

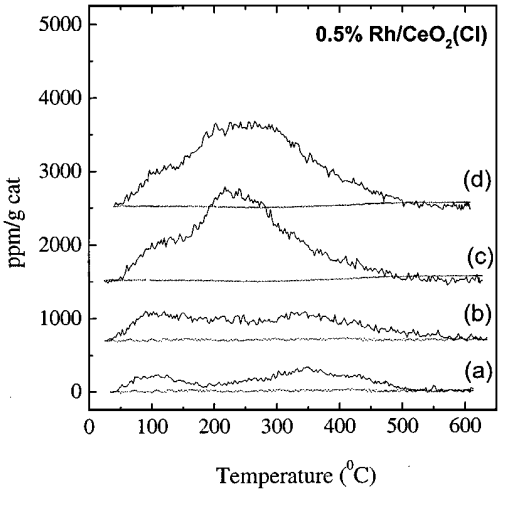

FIG. 4. TPD-MS spectra obtained following hydrogen adsorption on the 0.5% $Rh/CeO_2(Cl)$ catalyst for 30 min at temperatures of 25 (a), 100 (b), 200 (c), and 300°C (d). Solid lines, H_2; dotted lines, H_2O.

are observed, but the TPD spectra differ significantly from those obtained from the Cl-free Rh/CeO_2 sample. The total amount of the desorbed hydrogen increases with increasing adsorption temperature but is significantly lower (Table 3) than the corresponding quantity observed over the Cl-free catalysts for all adsorption temperatures examined (compare Figs. 3 and 4).

The low-temperature peak located at 100°C is not significantly affected by the presence of chlorine, although it is smaller than the corresponding one over the Cl-free sample. The main difference is the drastic decrease in the amount of the activated peak which was observed to desorb between 170 and 200°C from $Rh/CeO_2(N)$. Its relative intensity compared to that of the low-temperature peak is smaller than the corresponding one of the Cl-free sample; it is broader and its maximum is shifted toward higher desorption temperature, i.e., above 200°C. The high-temperature peak is also affected by the presence of chlorine; it is also decreased in intensity and cannot be discriminated from the peak originating from the activated hydrogen species.

In contrast to the Cl-free sample, no water is observed to desorb from this sample at the adsorption temperatures examined, indicating that either hydroxyl groups are not formed or they are strongly held on the surface and do not combine with adsorbed hydrogen atoms to yield water under the experimental conditions used. Results from the XPS experiments indicate that the former explanation is the most probable: no hydroxyl groups are observed on $Rh/CeO_2(Cl)$ in contrast to $Rh/CeO_2(N)$ where a significant amount of hydroxyl groups are present after reduction at 300°C.

CO Adsorption

(i) Unmetallized $CeO_2(N)$ and $CeO_2(Cl)$. TPD spectra obtained following CO chemisorption on $CeO_2(N)$, in the temperature range of 25 to 300°C, are shown in Fig. 5. After adsorption at 25°C, no CO is observed to desorb from ceria. Only a broad CO_2 band, which starts evolving at 350°C, is present in the TPD spectrum (Fig. 5a). Increasing adsorption temperature to 100°C results in the appearance of a small CO peak located at 300°C and in an increase of the amount of CO_2 which starts desorbing at ca. 300°C (Fig. 5b). The CO peak becomes clearly pronounced upon increasing adsorption temperature to 200 and 300°C (Figs. 5c and 5d). In addition, increasing CO adsorption temperature above 200°C results in the appearance of a second CO_2 band at about 250°C. The amounts of desorbed CO and CO_2 as a function of adsorption temperature are listed in Table 4.

On the contrary, similarly treated $CeO_2(Cl)$ catalyst did not exhibit the same behavior in the TPD experiments: Neither CO nor CO_2 was observed to desorb at the adsorption temperatures examined, indicating that the presence of chlorine on the ceria support significantly influences its chemisorptive properties by hindering CO interaction with ceria.

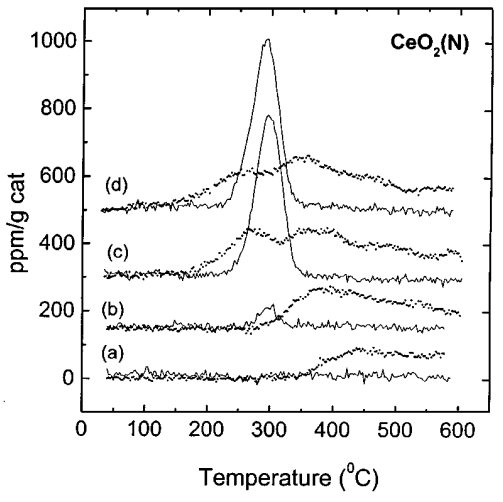

FIG. 5. TPD-MS spectra obtained following treatment of $CeO_2(N)$ with CO at temperatures of 25 (a), 100 (b), 200 (c), and 300°C (d). Solid lines, CO; dotted lines, CO_2.

(ii) Cl-free Rh/CeO_2. TPD-MS spectra obtained following CO chemisorption on Cl-free Rh/CeO_2 catalysts in the temperature range of 25 to 300°C are shown in Fig. 6. It is observed that CO and CO_2 desorb from the catalyst surface in quantities and temperatures which strongly depend on adsorption temperature.

When CO adsorption occurs at 25°C, a single CO peak is observed at around 100°C (Fig. 6a). CO_2 exhibits an intense peak at the same temperature followed by a broad CO_2 spectral feature which extends to 550°C. Increasing adsorption temperature to 100°C results in the appearance of a second CO peak, which appears as a high temperature shoulder, desorbing at around 150°C. This peak increases in intensity and shifts to higher desorption temperatures (200–250°C) upon increasing adsorption temperature to 200 and 300°C (Figs. 6c and 6d). In parallel, the intense peak of

TABLE 4

Amounts of CO and CO_2 Desorbed from the Cl-Free and Cl-Containing CeO_2 and Rh/CeO_2 Samples Following Carbon Monoxide Adsorption in the Temperature Range 25–300°C

	Amount of desorbed species (μmol/g cat)							
	$CeO_2(N)$		$CeO_2(Cl)$		$Rh/CeO_2(N)$		$Rh/CeO_2(Cl)$	
T_{ads} (°C)	CO	CO_2	CO	CO_2	CO	CO_2	CO	CO_2
25	—	1.70	—	—	0.38	6.70	0.89	1.88
100	0.22	1.21	—	—	0.67	7.59	1.29	2.23
200	1.43	2.5	—	—	0.98	6.34	1.22	2.99
300	1.65	2.54	—	—	1.03	8.30	1.65	3.05

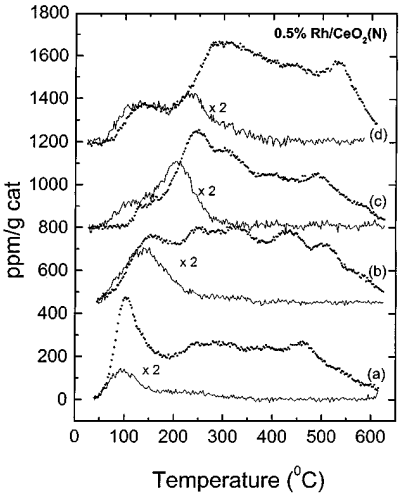

FIG. 6. TPD-MS spectra obtained following treatment of $Rh/CeO_2(N)$ with CO at temperatures of 25 (a), 100 (b), 200 (c), and 300°C (d). Solid lines, CO; dotted lines, CO_2.

CO_2 located at 100°C for $T_{ad} = 25$°C (Fig. 6a) is progressively lowered in intensity with increasing adsorption temperature, while the onset of the CO_2 desorbtion band shifts to higher temperatures (Figs. 6b–6d). The amounts of the desorbed species of Fig. 6 are listed in Table 4.

(iii) Cl-containing Rh/CeO_2. TPD spectra obtained after CO chemisorption on the Cl-containing 0.5% Rh/CeO_2 catalyst are shown in Fig. 7. These spectra differ markedly from the corresponding ones obtained from the Cl-free catalyst (Fig. 6). CO adsorption at room temperature leads to the appearance of three CO peaks located at about 100, 200, and 300°C, of which only the first appears in the corresponding spectrum of $Rh/CeO_2(N)$ (Fig. 6a). The peak at ~200°C can be correlated to the activated species observed to desorb at 150–250°C from $Rh/CeO_2(N)$, which was only present at adsorption temperatures above 100°C. The high-temperature CO peak at 300°C (Fig. 7a) was not observed over the Cl-free sample in the adsorption temperature range examined, indicating that its origin is related to the presence of chlorine on the surface of the catalyst. Concerning CO_2, it exhibits a very small peak at 100°C and an intense peak located at 300°C, accompanied by a high-temperature shoulder extending up to 500°C (Fig. 7a). The absence of the CO_2 peak at 100°C is the striking difference between Cl-containing (Fig. 7a) and Cl-free (Fig. 6a) Rh/CeO_2 samples.

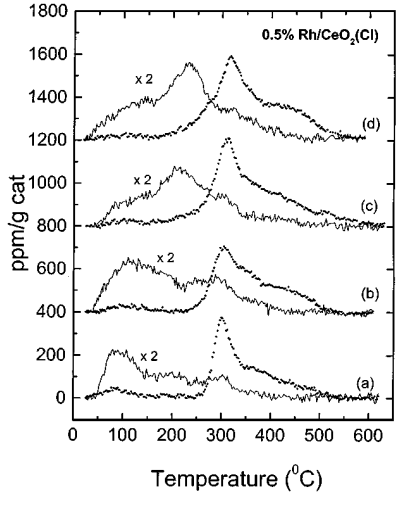

FIG. 7. TPD-MS spectra obtained following treatment of $Rh/CeO_2(Cl)$ with CO at temperatures of 25 (a), 100 (b), 200 (c), and 300°C (d). Solid lines, CO, dotted lines, CO_2.

Increasing adsorption temperature results in an increase of the amount of desorbed CO and in the pronounced appearance of the activated CO peak in the desorption temperature region of 200–250°C (Fig. 7), which is also the case for the Cl-free catalyst. Increasing adsorption temperature alters CO_2 curves quantitatively but not qualitatively: The amount of desorbing CO_2 increases upon increasing adsorption temperature, while, in contrast to the Cl-free sample, only minor amounts of CO_2 are produced at temperatures below 250°C. The amounts of desorbed CO and CO_2 as a function of adsorption temperature are listed in Table 4.

4. DISCUSSION

Hydrogen Adsorption on CeO_2 and Rh/CeO_2

The appearance of both H_2 and H_2O desorbing from $CeO_2(N)$ (Fig. 2) indicates that interaction of this sample with hydrogen at 300°C leads to both irreversible reduction of ceria, i.e., water formation, and reversible reduction, i.e., chemisorption of hydrogen, which can further be desorbed upon heating as H_2. According to TPR experiments reported in the literature (1), reduction of unmetallized CeO_2 surfaces begins at about 300°C, the reduction temperature employed in the present study, leading to a superficial reduction $Ce^{4+} \rightarrow Ce^{3+}$, whereas the mass reduction sets at much higher temperatures, ca. 800°C (1). The TPD curves observed in Fig. 2 indicate that hydrogen treatment at 300°C leads to partial reduction of the cerium oxide surface: Hydrogen dissociatively adsorbs on $CeO_2(N)$, forming hydroxyl groups. During the TPD experiments, hydrogen atoms either recombine to form H_2 or desorb as water after recombination with surface hydroxyl groups. Over $CeO_2(Cl)$ these steps occur to a lesser extent; higher reduction temperatures are probably needed to obtain the same results. The presence of chlorine on the surface seems to hinder hydrogen adsorption and formation of hydroxyl groups. The formation of hydroxyl groups upon treating ceria with hydrogen has been verified with FTIR experiments (9, 43), where it was found that their amount increases with increasing reduction temperature up to 400°C. Above this temperature, the corresponding ν(OH) band decreases in

intensity due to the thermally induced desorption of water. Apart from hydroxyl species, another form of hydrogen storage on ceria has been proposed by Fierro *et al.* (44, 45) and involves the formation of ceria "bronzes."

The presence of Rh dispersed on CeO_2 activates hydrogen and leads to the appearance of additional hydrogen adsorption species (Figs. 3 and 4). In the case of Cl-free Rh/CeO_2 (Fig. 3) three TPD peaks, located at ca. 110, 170, and 400°C, are observed following hydrogen adsorption at room temperature. The broad peak at 400°C evolves at the same temperature region as the species observed over bare CeO_2(N) (Fig. 2) and therefore can be attributed to hydrogen originating from the support. It is well known ((1) and references therein) that the presence of metal particles dispersed on ceria strongly favors hydrogen spillover on the support and that this spillover process leads to complete surface reduction of the oxide (6). The present XPS experiments (Fig. 1A, Table 2) show that an amount of cerium (4%) is reduced to Ce^{3+} upon interaction of Rh/CeO_2(N) with hydrogen at 300°C, which most probably is due to reduction of the upper surface cerium atoms. The rather low degree of reduction is due to the low surface area of ceria (3.6 m^2/g). The shift of the high-temperature TPD peaks, attributed to hydrogen adsorption on ceria, to lower temperatures upon increasing adsorption temperature (Fig. 3) could be due to back-spillover of hydrogen which has been found to occur at low temperatures, thus preventing a net separation between the desorption processes from the metal crystallites and those recorded at high temperatures, attributed to hydrogen interaction with the support.

Considering the nature of the two H_2 peaks with their maxima located at ca. 110 and 170–210°C, the former could be attributed to hydrogen adsorbed on bulk Rh (13), and the latter to hydrogen adsorbed on sites located at the metal–support interface (14). Ioannides and Verykios (14) examined the influence of the carrier (SiO_2, Al_2O_3, and TiO_2) on the interaction of supported Rh with H_2 and CO. TPD spectra of hydrogen revealed two modes of adsorption on Rh/Al_2O_3 and Rh/TiO_2, one of which was activated. Their TPD spectra consisted of two peaks at 70–100°C and 160–200°C, in accordance with the results of the present study. The activated mode was not observed over Rh/SiO_2. The activated, strongly adsorbed hydrogen species was attributed to hydrogen adsorbed on Rh located at the metal–support interface or to the creation of new adsorption sites on the surface of small Rh crystallites which is expected to have more defects than the Rh(111) surface (14). Apple *et al.* (15) also observed H_2 desorption peaks at 80 and 240°C after hydrogen chemisorption at 300°C, accompanied by a third peak at 540°C attributed to hydrogen spillover.

Production of water observed to occur during TPD experiments conducted following hydrogen adsorption at temperatures above 100°C (Fig. 3) indicates that the presence of Rh favors irreversible reduction of CeO_2(N) at lower temperatures. It should be recalled that water was not produced over bare CeO_2(N) at temperatures below 300°C (Fig. 2). These observations indicate that oxygen from CeO_2(N) is removed more easily in the presence of rhodium, possibly due to oxygen migration from the support to the metal particles. This is in accordance with the work of Zafiris and Gorte (32), who found evidence that oxygen from ceria can migrate onto Rh and react with adsorbates on the Rh, starting at approximately 130°C.

The presence of chlorine on the catalyst surface strongly influences the properties of Rh/CeO_2(Cl) toward hydrogen adsorption (Fig. 4). The most important difference between the Cl-free (Fig. 3) and the Cl-containing (Fig. 4) catalysts is the drastic decrease in the population of the activated species which, depending on adsorption temperature, desorbs between 150 and 250°C. This species is attributed to hydrogen adsorbed on sites located at the metal–support interface. This can be explained by taking into account that chlorination of the carrier withdraws electrons from the Rh particles and therefore lowers the capacity of the metal to adsorb hydrogen. This phenomenon is expected to be more important in the vicinity of the metal–support interface, where the activated hydrogen adsorption process occurs (compare Figs. 3 and 4). Furthermore, XPS experiments showed that a significant amount of Rh^{3+} species is present on Rh/CeO_2(Cl) (Fig. 1C). These species are probably located in the metal–support interface, associated with chloride ions of the support, thus hindering adsorption of the activated hydrogen species on these sites.

Differences of metal dispersion of Rh on the Cl-free and the Cl-containing Rh/CeO_2 catalysts may also be responsible for the observed differences in the TPD spectra of Figs. 3 and 4. The XPS results presented in Table 1 indicate that the Rh dispersion of the Cl-containing catalyst is rather poor, since the Cl : Rh atomic ratio is 7.1 : 0.7, much larger than that expected for highly dispersed rhodium which, assuming that all chlorine is trapped by the support, should give a ratio of 3 : 1.

The high-temperature peak attributed to hydrogen adsorption on the support is also affected by the presence of chlorine; it decreases in intensity and cannot be discriminated from the peak originating from the activated hydrogen species due to overlapping with the activated species mentioned above. It is known that chlorine hinders hydrogen adsorption on the support via spillover processes (8, 34). It has been shown that the use of rhodium chloride as the metal precursor blocks the spillover process. Bernal *et al.* (8) concluded that the use of $RhCl_3$ as the metal precursor disturbs the mechanism of hydrogen transfer from the metal to the support and the chemisorptive properties of the support itself to a much larger extent than the chemical properties of the metal. Fajardie *et al.* (34) attributed the absence of hydrogen spillover during chemisorption measurements over Cl-containing catalyst to the substitution

of the ceria lattice oxygen ions by Cl^- due to the use of $RhCl_3 \cdot 3H_2O$ as metal precursor. A relative inhibition of hydrogen spillover was also observed by the same authors when the temperature of reduction was increased from 300 to 500°C. This phenomenon was attributed to the decrease in the number of hydroxyl groups which are believed to play an important role in the spillover mechanism. Indeed, our experiments of hydrogen adsorption on unmetallized CeO_2 (Fig. 2) show that water desorption from the Cl-containing sample is much lower in quantity compared to Cl-free CeO_2. Similar are the results from the Rh/CeO_2 catalysts, where it is observed that water is produced only over the Cl-free sample (Fig. 3) and not over the Cl-containing sample (Fig. 4), indicating the absence of hydroxyl groups formed on the surface of the latter, which is suggested by the present XPS experiments (Fig. 1B).

Comparison of the TPD spectra obtained from bare (Fig. 2) and metallized (Figs. 3 and 4) CeO_2 samples indicates that the presence of Rh modifies the support qualities by activating hydrogen, which leads to surface reduction of cerium oxide. Therefore, the treatment of Rh-containing ceria catalysts with hydrogen leads to more important surface reduction, as compared to the bare ceria surfaces, even at temperatures lower than 300°C. Hydrogen activated by precious metal can easily spillover onto the support at low adsorption temperatures. This phenomenon has been described in several studies on the adsorption of hydrogen on precious-metal-type solids deposited on cerium oxides (6, 7, 46) and is also observed in the present study.

In the present experiments, when chlorine exists on unmetallized ceria, hydrogen adsorption takes place to a much lesser extent. The same is true for Rh-containing catalysts: The hydrogen chemisorption capacity of the Cl-containing catalysts is significantly suppressed and the relative population of the adsorbed species is changed. It is also interesting to note that no water is observed in the TPD spectra of $Rh/CeO_2(Cl)$, indicating that irreversible adsorption of hydrogen on ceria does not take place. It may be assumed that the presence of chlorine hinders oxygen migration from the support to Rh and the concomitant creation of oxygen vacancies. This would imply significant alternations in the catalytic properties of Cl-containing M/CeO_2 catalysts, since the catalytic properties of ceria are often related to its ability to store and release oxygen, acting as a regulator of the oxygen partial pressure over the catalyst. Bernal *et al.* (47) suggested that the presence of chlorine in the catalyst strongly modifies redox behavior of ceria. The authors observed that hydrogen treatment of Cl-containing Rh/CeO_2 samples at 350°C leads to an almost irreversible reduction of ceria (47) but the presence of Ce^{3+} species does not necessarily imply the existence of oxygen vacancies. Although a much deeper irreversible reduction occurs, reoxidation of ceria becomes much slower with concomitant influence in its catalytic properties.

CO Adsorption on CeO_2 and Rh/CeO_2

The TPD spectra of Fig. 5 obtained following adsorption of CO on $CeO_2(N)$ in the temperature range of 25 to 300°C show that Cl-free ceria interacts with carbon monoxide, yielding both CO and CO_2 in subsequent thermal desorption experiments. On the contrary, neither CO nor CO_2 is observed on similar experiments conducted over $CeO_2(Cl)$, indicating that the presence of chlorine hinders interaction of ceria with carbon monoxide.

CO is known to adsorb on coordinatively unsaturated metal cations (Lewis acid cites) formed by the removal of certain OH groups. Li *et al.* (43) reported that surface unsaturated sites on CeO_2 can be generated by dehydroxylation at high temperatures and that these sites are vital to the activation of CO to form carbonate and inorganic carboxylate species. It should be recalled that, in the present experiments, an oxidation/reduction cycle preceded CO adsorption followed by heating to 600°C under He flow. The latter step of this pretreatment process results in partial dehydroxylation of the surface as observed in the H_2-TPD experiments over $CeO_2(N)$ (Fig. 2) and in the concomitant creation of coordinatively unsaturated sites on the ceria surface. It may then be assumed that it is on these surface sites that CO adsorbs, giving rise to the spectral features observed in Fig. 5.

Concerning the nature of the adsorbed species, it is known that CO adsorption on clean CeO_2 surfaces yields linearly adsorbed CO, carbonates, and carboxylates (48). Linear CO adsorption is favored over Ce^{3+} ions generated after hydrogen reduction probably due to a slight retrodonation from Ce^{3+} to CO (48). The CO TPD peaks observed in Fig. 5 could then be attributed to linear CO adsorbed on Ce^{3+}. For ceria, carbon monoxide is a better reducing agent than hydrogen. It is known that in the presence of CO, reduction of surface oxygen of CeO_2 with formation of oxygen vacancies and CO_2 readily occurs even at room temperature, while stoichiometries close to $CeO_{1.94}$ and $CeO_{1.86}$ are observed at 300 and 400°C, respectively (1). It is therefore expected that treatment of ceria with CO in the temperature range examined results in significant reduction of the ceria surface in a degree depending on CO adsorption temperature; i.e., higher temperature will result in greater surface reduction. If so, the amount of Ce^{3+} ions increases with increasing CO adsorption temperature and the population of linear-CO species is also expected to increase, in accordance with the TPD spectra of Fig. 5. During reduction of CeO_2 by CO, carbonates and carboxylates are also formed. These species decompose upon heating during TPD and may be responsible for the observed CO_2 TPD curves (Figs. 5a and 5b). CO_2 may also be produced by disproportionation of CO to C and CO_2, especially at elevated temperatures, a process that could lead to the production of the additional CO_2 curve

observed after CO adsorption at 200 and 300°C (Figs. 5c and 5d).

It is worth noticing that neither CO nor CO_2 desorbs in the TPD experiments following CO interaction with CeO_2(Cl) in the examined adsorption temperature range. This implies that CO does not interact with chlorinated ceria surfaces or that this interaction produces surface species that do not desorb upon heating to 600°C during TPD. The absence of CO interaction with Cl-containing ceria is probably the case here. If oxygen vacancies are needed to stabilize CO adsorption, the occupancy of such sites by chlorine could hinder adsorption. It is generally believed that CO does not adsorb over chlorinated ceria (34). This is why conventional static equilibrium methods are applicable to Cl-containing ceria samples. It should also be mentioned that carboxylate and bidenate entities are preferentially formed on surfaces prereduced with hydrogen (48). Hydrogen adsorption experiments presented in a previous section imply that unmetallized Cl-containing ceria samples do not interact with hydrogen at 300°C (Fig. 2), the reduction temperature employed in the present study, providing an additional reason for the absence of interaction between CO and Cl-containing samples. Badri *et al.* (5) studied CO adsorption on surface chlorinated ceria and Cl-containing reduced Pd/CeO_2 catalysts at room temperature, employing FTIR. The reduced Pd/CeO_2 catalyst was found to be unreactive toward CO. For Cl-free Pd/CeO_2 samples, formate species were produced upon adsorbing CO. Metal sites were found not to be necessary for the production of formate species in H_2-reduced ceria, but special sites were needed, like the monodentate surface hydroxyl species. Chlorination of such sites would prevent formate formation (5). The absence of hydroxyl groups could be responsible for the absence of interaction between CeO_2(Cl) and CO.

As in the case of hydrogen TPD experiments, it is observed that the presence of chlorine alters the chemisorption properties of the CeO_2 surface by reducing its chemisorptive capacity for CO adsorption.

Carbon monoxide adsorption on Rh/CeO_2 catalysts results in the appearance of several CO and CO_2 peaks in the TPD spectra for both Cl-free (Fig. 6) and Cl-containing (Fig. 7) samples. TPD spectra obtained from CO adsorbed on Rh dispersed on high-surface-area carriers are significantly more complex than the corresponding ones over model catalysts. Both CO and CO_2 peaks are observed to desorb (19, 20), as in the present experiments.

Extensive infrared studies of carbon monoxide adsorption on supported rhodium established the existence of at least three CO species in the adsorbed mode: linear- and bridge-bonded CO on Rh^0 sites and dicarbonyl species on dispersed Rh^+ sites (21–23). CO chemisorption on Rh sites is a fairly fast process and the appearance of gem-dicarbonyl bands usually takes place after those of linear- and bridge-bonded CO on Rh^0 sites (26, 27, 49, 50). Upon thermal desorption, initially formed dicarbonyls are transformed to linear- and bridge-bonded CO on Rh^0 and the CO desorption sequence occurs in the following order: $Rh(CO)_2 > Rh_2(CO) > Rh(CO)$ (19).

CO desorbs from Rh deposited on amorphous CeO_2, yielding two CO peaks at 140 and 200°C due to linear and bridged CO, while CO_2 is also produced following interaction of CO with oxygen originating from the ceria (32). Formation of another, strongly bonded CO species obtained from Rh supported on partially reduced CeO_2 surfaces has also been reported (33) and has been attributed to the desorption of CO which is bridge-bonded between Rh and Ce^{3+} cations on the ceria support.

The CO peaks observed at 100 and 200–250°C from Rh/CeO_2 (N) (Fig. 6) could be attributed to the desorption of initially formed dicarbonyl species and to desorption of linear and bridged forms of CO. The low-temperature intense CO_2 peak observed in the TPD spectra obtained after CO adsorption on Rh/CeO_2(N) at 25°C (Fig. 6a) can be attributed to adsorbed CO oxidized to CO_2 by oxygen originating from ceria and/or oxygen produced by CO dissociation; reduction of CeO_2 by CO is known to occur at low temperatures. Zafiris and Gorte found evidence that oxygen from CeO_2 can migrate onto Rh and react with adsorbates on the Rh beginning at ~130°C (32, 51). Similarly, Jin *et al.* (30) concluded that carbon dioxide formed in the TPD experiments conducted following CO adsorption on Pt/CeO_2 catalysts is produced from the reaction of adsorbed CO with a lattice oxygen atom of ceria. The structure of CeO_2 has been found to influence the rate of oxygen transfer from the support to the Rh particles (33, 50, 52). The rate of oxygen migration from ceria to supported Rh seems to depend on the crystallographic orientation of the oxide support, while oxygen diffusion is significantly higher in polycrystalline CeO_2.

As the intense CO_2 peak at 100°C evolves simultaneously with the CO species adsorbed on Rh particles (Fig. 6a) it can be assumed that it originates from the same adsorbed species, i.e., CO adsorbed on Rh sites. Part of this species desorbs as CO while most of it interacts with oxygen migrated from the ceria surface to yield CO_2. Considering the origin of oxygen which reacts with adsorbed CO, it most possibly is "surface capping" oxygen of the ceria support. As observed in Fig. 6, increasing adsorption temperature results in the decrease of the low-temperature CO_2 peak and in a shift of the initiation of the CO_2 broad band at temperatures comparable to those at which adsorption of CO took place. For example, after CO adsorption at 100°C, CO_2 starts evolving above this temperature (Fig. 6). This can be explained as follows: At adsorption temperatures higher than room temperature, a reaction between CO and CeO_2 rather than CO adsorption takes place. A significant amount of CO_2 is produced during CO adsorption

and subsequent interaction with surface capping oxygen of ceria, leading to oxygen depletion of the ceria surface and to the concomitant absence of the corresponding intense CO_2 peak. Further increasing CO adsorption temperature leads to depletion of oxygen anions originating from the bulk of ceria, since diffusion of oxygen is favored at elevated temperatures. The existence of small amounts of CO_2 in the temperature region below 200°C, even after CO adsorption at 200 or 300°C (Fig. 6), can be attributed to replacement of reacted surface oxygen atoms by diffusion from the bulk ceria lattice during cooling to room temperature.

Concerning the broad CO_2 band observed to desorb in the temperature range of 200 to 600°C, it can be attributed to species originating from the ceria surface. As observed in Fig. 5, amounts of CO_2 desorb from unmetallized CeO_2(N) following CO adsorption at all temperatures examined, which can be attributed to the formation of carbonate species and/or to the disproportionation of CO. The broad CO_2 band of Fig. 6 can also be attributed to the same species. It is also possible that part of the CO_2 produced in the TPD experiments is due to dissociation of CO on rhodium. Solymosi and Erdohelyi (19, 20) first established that dissociation of CO on supported Rh catalysts occurs at temperatures above 200°C.

The striking difference between the CO_2 curves obtained from the Cl-free and the Cl-containing 0.5% Rh/CeO_2 catalysts is that for the latter no CO_2 is desorbed at temperatures lower than 250°C. It is evident that carbon monoxide adsorbed on Rh is not oxidized by the ceria support to yield CO_2 as in the case of Cl-free catalysts and only desorbs as CO. No CO_2 is produced in this temperature range, as oxygen transfer from CeO_2 to Rh–CO is hindered due to the presence of chlorine. As discussed above, chlorination by the impregnation method followed by ORC during pretreatment gives rise to some lattice O^{2-} exchange with Cl^- ions forming $Ce^{(III)}OCl$ (3–5). If this is so, the presence of chlorine on the Rh/CeO_2 catalyst is expected to hinder the further reduction of ceria and formation of oxygen vacancies and, consequently, its oxygen storage and release capacity which improves the performance of three-way catalysts under fuel-lean and fuel-rich conditions, respectively.

Of particular interest is the appearance of the new, strongly adsorbed CO species on the Rh/CeO_2(Cl) catalyst, populated even at room temperature and desorbing at ca. 300°C in the TPD spectra (Fig. 7), which is absent in the corresponding spectra obtained from the Rh/CeO_2(N) catalyst. The CO_2 peak observed to desorb at the same temperature can also be assumed to originate from this strongly held CO species which at these high temperatures (i.e., above 250°C) reacts with oxygen originating from the CeO_2(Cl) support to yield CO_2. It can also be attributed to dissociation of irreversibly adsorbed CO.

The origin of the high-temperature CO peak, which was observed only over the Cl-containing catalyst, can be connected to the presence of chlorine on the ceria surface and possibly to the presence of rhodium in the Rh^{3+} oxidation state. It is well known that the electronic state of supported rhodium catalysts influences catalytic properties, as for example selectivity of CO hydrogenation for production of oxygen-containing products (42). Since an assignment of the CO peak at 300°C cannot be made based on only the TPD-MS experiments of the present study, the adsorption and desorption characteristics of CO on the Rh/CeO_2(Cl) will be studied further employing FTIR and XPS and will be presented in a future publication.

5. CONCLUSIONS

(1) Rh/CeO_2 catalysts prepared using $RhCl_3 \cdot H_2O$ as the metal precursor retain a significant amount of Cl species on the ceria surface (~7 at%) after reduction with hydrogen at 300°C, while a large amount of cerium (~30%) exists in the Ce^{3+} oxidation state, probably due to the formation of cerium oxychloride ($Ce^{(III)}OCl$).

(2) For unmetallized ceria, the presence of chlorine hinders the reversible chemisorption of hydrogen and the formation of hydroxyl groups upon treatment with hydrogen, and diminishes its chemisorption capacity for CO adsorption.

(3) Following reduction with hydrogen at 300°C, Rh^0 and Rh^+ sites coexist on both Cl-free and Cl-containing Rh/CeO_2 catalysts, while Rh^{3+} species are also present on Rh/CeO_2(Cl).

(4) Three hydrogen species are observed to desorb from Rh/CeO_2(N), attributed to hydrogen adsorbed on bulk Rh, to hydrogen adsorbed on Rh atoms located at the metal–support interface, and to hydrogen adsorption on the ceria support, following a spillover process. The presence of chlorine hinders hydrogen adsorption and significantly lowers the population of the species adsorbed at the metal–support interface.

(5) Carbon monoxide desorbs from Rh/CeO_2(N) catalyst, giving two CO peaks at 100 and 150–210°C, followed by large amounts of CO_2 produced after interaction of adsorbed CO with oxygen originating from the ceria support. The presence of chlorine leads to a drastic decrease of produced CO_2, indicating that oxygen migration from chlorinated ceria surfaces is hindered. An additional, strongly held CO species, possibly associated to Rh^{3+} sites, is also observed, desorbing at 300°C.

(6) The presence of chloride on the Rh/CeO_2 catalysts induces alterations to the redox behavior of ceria and the chemisorptive properties of rhodium which are expected to significantly alter the catalytic properties of Rh/CeO_2 toward CO oxidation and CO hydrogenation reactions.

ACKNOWLEDGMENT

The authors thank Dr. S. Neophytides of the Institute of Chemical Engineering and High Temperature Chemical Processes (ICE/HT) for his kind assistance with the XPS measurements.

REFERENCES

1. Trovarelli, A., *Catal. Rev. Sci. Eng.* **38**, 439 (1996).
2. Engler, B., Koberstein, E., and Schubert, P., *Appl. Catal.* **48**, 71 (1989).
3. Le Normand, F., Hilaire, L., Kili, K., Krill, G., and Maire, G. J., *Phys. Chem.* **92**, 2561 (1988).
4. Kepinski, L., Wolcyrz, M., and Okal, J. J., *Chem. Soc. Faraday Trans.* **91**, 507 (1995).
5. Badri, A., Binet, C., and Lavalley, J. C., *J. Phys. Chem.* **200**, 8363 (1996).
6. Bernal, B., Calvino, J. J., Cifredo, G. A., Rodriguez-Izquierdo, J. M., Perrichon, V., and Laachir, A., *J. Catal.* **137**, 1 (1992).
7. Bernal, S., Botana, F. J., Garcia, R., Kang, Z., Lopez, M. L., Pan, M., Ramirez, F., and Rodriguez-Izquierdo, J. M., *Catal. Today* **2**, 653 (1988).
8. Bernal, S., Botana, F. J., Calvino, J. J., Cauqui, M. A., Cifredo, G. A., Jobacho, A., Pintado, J. M., and Rodriguez-Izquierdo, J. M., *J. Phys. Chem.* **97**, 4118 (1993).
9. Bernal, S., Calvino, J. J., Cifredo, G. A., Gatica, J. M., Omil, J. A. P., and Pintado, J. M., *J. Chem. Soc. Faraday Trans.* **89**, 3499 (1993).
10. Trovarelli, A., de Leitenburg, C., and Dolcetti, G. J., *Chem. Soc. Chem. Commun.*, 472 (1991).
11. Trovarelli, A., Dolcetti, G., de Leitenburg, C., Kaspar, J., Finetti, P., and Santoni, A. J., *Chem. Soc. Faraday Trans.* **88**, 1311 (1992).
12. de Leitenburg, C., and Trovarelli, A., *J. Catal.* **156**, 171 (1995).
13. Yates, J. T., Thiel, P. A., and Weinberg, W. H., *Surf. Sci.* **84**, 427 (1979).
14. Ioannides, T., and Verykios, X. E., *J. Catal.* **140**, 353 (1993).
15. Apple, T. M., Cajardo, P., and Dybowski, C., *J. Catal.* **68**, 103 (1981).
16. Mate, C. M., and Somorjai, G. A., *Surf. Sci.* **160**, 542 (1985).
17. Bertel, E., Rosina, G., and Netzler, F. R., *Surf. Sci.* **172**, L515 (1986).
18. Marbrow, R. A., and Lambert, R. M., *Surf. Sci.* **67**, 489 (1997).
19. Solymosi, F., and Erdohelyi, A., *Surf. Sci.* **110**, L630 (1981).
20. Erdohelyi, A., and Solymosi, F., *J. Catal.* **84**, 446 (1983).
21. Yang, A. C., and Garland, C. W., *J. Phys. Chem.* **61**, 1504 (1957).
22. Yates Jr., J. T., Duncan, T. M., and Vaughan, R. W., *J. Chem. Phys.* **71**, 3908 (1979).
23. Rice, C. A., Worley, S. D., Curtis, C. W., Guin, J. A., and Tarrer, A. R., *J. Chem. Phys.* **74**, 6487 (1981).
24. Trautmann, S., and Baerns, M., *J. Catal.* **150**, 335 (1994).
25. Van't Blik, H. F. J., Van Zon, J. B. A. D., Huizinga, T., Vis, J. C., Koningsberger, D. C., and Prins, R., *J. Phys. Chem.* **87**, 2264 (1983).
26. Solymosi, F., and Pasztor, M., *J. Phys. Chem.* **89**, 4789 (1985).
27. Basu, P., Panayotov, D., and Yates, J. T., Jr., *J. Phys. Chem.* **91**, 3133 (1987).
28. Bergeret, G., Gallezot, P., Gelin, P., Ben Taarit, Y., Lefebvre, F., Naccache, C., and Shannon, R. D., *J. Catal.* **104**, 279 (1987).
29. Jin, T., Okumura, T., Mains, G. T., and White, J. M., *J. Phys. Chem.* **91**, 3310 (1987).
30. Jin, T., Zhou, Y., Mains, G. T., and White, J. M., *J. Phys. Chem.* **91**, 5931 (1987).
31. Zhou, Y., Nakashima, M., and White, J. M., *J. Phys. Chem.* **92**, 812 (1988).
32. Zafiris, G. C., and Gorte, R. J., *J. Catal.* **139**, 561 (1993).
33. Stubenrauch, J., and Vohs, J. M., *J. Catal.* **159**, 50 (1996).
34. Fajardie, F., Tempere, J. F., Djega-Mariadassou, G., and Blanchard, G. J., *J. Catal.* **163**, 77 (1996).
35. Briggs, D., and Seah, M. P., Eds., "Practical Surface Analysis, Vol. 1: Auger and X-Ray Photoelectron Spectroscopy," Appendix 6. Wiley, New York, 1990.
36. Efstathiou, A. M., Papageorgiou, D., and Verykios, X. E., *J. Catal.* **141**, 612 (1993).
37. Fujimori, A., *Phys. Rev. B* **28**, 2281 (1983).
38. Shyu, J. Z., Weber, W. H., and Gandi, H. S., *J. Phys. Chem.* **92**, 4964 (1988).
39. Creaser, D. A., Harisson, P. G., Morris, M. A., and Wolfindale, B. A., *Catal. Lett.* **23**, 13 (1994).
40. Qiu, S. L., Lin, C. L., Chen, J., and Slrongin, M., *Phys. Rev. B* **41**, 7467 (1990).
41. Baltanas, M. A., Onuferko, J. H., McMillan, S. T., and Katzer, J. R., *J. Phys. Chem.* **91**, 3772 (1987).
42. Kawai, M., Uda, M., and Ichikawa, M., *J. Phys. Chem.* **89**, 1654 (1985).
43. Li, C., Sakata, Y., Arai, T., Domen, K., Maruya K., and Onishi, T., *J. Chem. Soc. Faraday Trans.* **85**, 1451 (1989).
44. Fierro, J. L. G., Soria, J., Sanz, J., and Rojo, J. M., *J. Solid State Chem.* **66**, 154 (1987).
45. Cunningham, J., O'Brien, S., Sanz, J., Rojo, M., Soria, J. A., and Fierro, J. L. G., *J. Mol. Catal.* **57**, 379 (1990).
46. Tournayan, L., Marcillio, N. R., and Frety, R., *Appl. Catal.* **31**, 78 (1991).
47. Bernal, S., Calvino, J. J., Gifredo, G. A., and Rodriquez-Izquierdo, J. M., *J. Phys. Chem.* **99**, 11794 (1995).
48. Bozon-Verduraz, F. A., and Bensalem, A., *J. Chem. Soc. Faraday Trans.* **90**, 653 (1994).
49. Zhang, Z. L., Kladi, A., and Verykios, X. E., *J. Mol. Catal.* **89**, 229 (1994).
50. Zhang, Z. L., Kladi, A., and Verykios, X. E., *J. Phys. Chem.* **98**, 6804 (1994).
51. Zafiris, G. S., and Gorte, R. J., *J. Catal.* **143**, 86 (1993).
52. Cordatos, H., Bunluensin, T., Stubenrauch, J., Vohs, J. M., and Gorte, R. J., *J. Phys. Chem.* **100**, 785 (1996).